Evidencing early pyrochlore formation in rare-earth doped TiO_2 nanocrystals: Structure sensing via VIS and NIR Er^{3+} light emission

I. Camps[1,6], M. Borlaf[2,4], J. Toudert[1,5], A. de Andrés[3], M. T. Colomer[2], R. Moreno[2] and R. Serna[1,7].

[1] *Instituto de Óptica, IO-CSIC, Serrano 121, 28006, Madrid, Spain.*

[2] *Instituto de Cerámica y Vidrio CSIC, Kelsen 5, 28049, Madrid, Spain.*

[3] *Instituto Ciencia de Materiales de Madrid, CSIC, Sor Juana Inés de la Cruz 3, Cantoblanco, 28049, Madrid, Spain.*

[4] *Present address: Laboratory for High Performance Ceramics, Empa, Überlandstrasse 129, 8600 Dübendorf, Switzerland*

[5] *Present address: Institut de Ciencies Fotoniques (ICFO), Barcelona Institute of Technology, 08860 Castelldefels (Barcelona), Spain*

[6] *ivancampsb@gmail.com*

[7] *rosalia.serna@csic.es*

Abstract

Er^{3+} doping of TiO_2 colloidal nanocrystals enhances their performance for photo-induced applications. Such doping is known to delay the anatase to rutile transformation under thermal treatment; nonetheless relevant information on the Er^{3+} light emission and location within the TiO_2 structures is still incomplete. Er^{3+} photoluminescence emission both in the visible (upconverted) and infrared photoluminescence is used for the first time to probe the ions location within the different TiO_2 structures. The results show that Er^{3+} ions in the as-prepared xerogels are not embedded in the anatase crystallites, and only upon thermal treatment Er^{3+} diffusion is induced into crystal

interstitial positions to form a solid solution. At higher temperatures rutile is formed inducing Er^{3+} segregation and giving rise to the formation of pyrochlore ($Er_2Ti_2O_7$), as shown by a distinct emission in the infrared spectrum due to the Er^{3+} ions located within the pyrochlore compound. Although pyrochlore is usually a high temperature phase, analysis of the photoluminescence allows its labeling at temperatures as low as 600-700 ºC for small Er^{3+} concentrations (1 mol %). Increasing Er^{3+} concentration promotes its enrichment at the nanocrystallites surface accomplished by the anatase-to-rutile phase transformation, suggesting that Er^{3+} ions control the TiO_2 nanocrystals surface properties.

Introduction

Due to its high chemical stability, low toxicity and excellent electrical and optical properties, titanium dioxide (TiO_2) is the target of intense research for many applications that span from catalytic applications (photocatalysis and water splitting) [1] to opto- and photoelectronic devices (LEDs and solar cells) [2]. In particular, TiO_2 is considered to be an excellent host for light emission applications in the visible and infrared, due to its wide optical bandgap (3.0 eV for rutile, 3.2 eV for anatase), wide transparency range and large refractive index (~2.5-3.0). Furthermore, the relatively low phonon energy of TiO_2 (<700 cm^{-1}) makes it especially suitable for the incorporation of optically active rare-earth ions such as Er^{3+}. The low phonon energy is necessary to prevent fast non-radiative de-excitations of the rare-earth ions through the phonons of the matrix, thus allowing to achieve high luminescence quantum yields required to light amplifiers [3,4], LEDs [5,6] and fluorophores [7]. Interestingly, doping of TiO_2 with a few percent of rare-earth ions (La^{3+}, Pr^{3+}, Nd^{3+},Eu^3, Gd^{3+}, Tb^{3+}, Dy^{3+}, Er^{3+}) has been also studied for a very different aim, since it has been shown that this incorporation is a

suitable procedure to stabilize the TiO_2 anatase phase [8,9], contrary to incorporations of specific materials that might induce the phase transformation, i.e. Fe:TiO_2 [10]. Particularly, for the case of lanthanide doped nanocrystalline TiO_2 xerogels produced by sol-gel, it has been shown that the rare-earth doping significantly retards the anatase-to-rutile phase transformation, stabilizes the mesoporous structure and delays the reduction of surface area of nanosized TiO_2 at high temperatures [11]. All these properties being useful for an enhanced catalysis performance. Therefore, there have been two main separate lines of investigation involving the rare earth doping of TiO_2, one focused to the optical performance and other dedicated to the structural characterization. However, in order to develop the full potential of rare earth-doped TiO_2 colloidal nanocrystalline materials for the different envisaged applications, a good understanding and control of their structure related to its optical performance is needed.

Within this context, for the case of Er^{3+}-doped TiO_2 it has been already shown that the colloidal sol-gel synthesis of TiO_2 provides an easy and robust route for the preparation of nanocrystalline rare-earth-doped TiO_2 sols, and we have already successfully produced high quality thin film from these colloids by electrophoretic deposition (EPD) for the case of Er-doped TiO_2[12], and by matrix laser assisted laser evaporation (MAPLE) for the case of Eu-doped TiO_2 [13]. Furthermore, the anatase to rutile phase transformation of the TiO_2 colloidal xerogels, as a function of the thermal treatment temperature and of the Er^{3+} doping was investigated using X-ray thermo- diffractometry (XRTD), complemented by transmission electron microscopy techniques [14]. It was found that indeed the presence of Er^{3+} ions in the nanocrystals induces a lower rate of anatase nanocrystalline growth, lower expansion, higher onset temperatures of the phase transformation and a slower kinetics of the anatase-to-rutile phase transformation. These results were associated with the formation of an interstitial solid solution of the Er^{3+}

ions within the anatase host[9,14]. In the present work, we aim to correlate the functional optical response of the obtained xerogels to their structural properties, as they undergo the anatase to rutile phase transformation, in order to identify the Er^{3+} location within the different formed crystalline structures. For this purpose, we perform a full optical characterization of the xerogels (UV-VIS-NIR spectroscopy and VIS-NIR photoluminescence), and a detailed Raman spectroscopy analysis to achieve their structural characterization, since previous works have demonstrated that Raman is a suitable and powerful tool to follow the kinetics of the phase transformation of TiO_2 colloidal nanoparticles [15]. Both the Er^{3+} visible emission resulting from upconversion excitation in the infrared, and Er^{3+} infrared emission around 1.53 μm resulting from direct visible excitations have been investigated. Since the shape of the light emission spectra is influenced by the local environment of the Er^{3+} ions, it is shown how their features evolve as the phase transformation progresses. It will be shown that the infrared emission, that has been usually neglected, in this case provides relevant and useful information, showing that it can be very sensitive to the formation of low concentration crystalline phases such as pyrochlore when Er^{3+} ions form part of their structure. The results presented in this work can be relevant for photon-induced applications, such as photo-induced catalysis that mainly relies in visible excitation.

Experimental procedure

The Er^{3+}-doped TiO_2 sols were synthesized in-house by colloidal sol–gel method. In a typical synthesis procedure, the alkoxide hydrolysis was carried out by adding, under continuous stirring, titanium (IV) isopropoxide (TIPO, 97 %, Sigma-Aldrich, Steinheim, Germany) to a mixture of deionized water (18.2 MΩ cm^{-1}, ultra-pure Milli-Q, France) and nitric acid (65 %, PANREAC, Barcelona, Spain) as a catalyst and

dispersing agent, with water/alkoxide molar ratio of 50 and H^+/Ti^{4+} of 0.2. For the preparation of the Er^{3+}-doped TiO_2 sols, erbium (III) acetate hydrate ($Er(OOCCH_3)_3 \cdot xH_2O$, Sigma-Aldrich, Steinheim, Germany) was first dissolved in the mixture of water and nitric acid to a molar relation Er^{3+}:Ti^{4+} of 1, 2 and 3 %, followed by the addition of the alkoxide. The synthesis temperature was maintained constant during the entire process at 35 ºC. Xerogels were subsequently obtained by drying the corresponding sols under ambient conditions of temperature and relative humidity. After drying, the xerogels were thermally annealed from 300 to 900 ºC, in steps of 100 ºC in air for 1 hour. The micro-Raman system consisting on a Jobin-Yvon HR 460 monochromator, liquid nitrogen cooled CCD and Kaiser Super-Notch-Plus filter to suppress the elastic scattered light at 488 nm was used to carry out Raman scattering measurements at room temperature. The excitation light (488nm line of an Ar^+–Kr^+ laser) was focused on the samples with an Olympus microscope and a x100 objective, which was also used to collect the scattered light. The absorption characteristics in a near-ultraviolet to near-infrared range of the Er^{3+}:TiO_2 nanocrystalline xerogels were studied by diffuse reflectance spectroscopy using a Varian Cary 5000 UV-Vis spectrometer coupled with an integration sphere accessory. PL measurements were carried out under excitation at λ = 488 nm at a nominal power of 36 mW from an Ar^+ ion laser (Spectra-Physics 2020-30) and, λ = 980 nm at a nominal power of 150 mW from a Ti:Sapphire laser (Spectra-Physics 3900S) pumped with the second harmonic of a Millennia Nd:YAG laser (λ = 532 nm). Appropriate amount of xerogel material was used in the PL experiments in order to fully absorb the excitation photons and to avoid spurious signal from the substrates or system holders; this procedure also allows us to compare the relative intensity of the acquired spectra. The light emitted by the samples was collected with a Czerny-Turner type monochromator (Acton Spectra Pro 300i, with

diffraction gratings of 300 and 1200 g/mm in the IR and the visible range, respectively) and detected through a Hamamatsu H10330B-75 PMT for the infrared emission, and an EMI 9659-QB for the visible emission. The signal was amplified with the standard lock-in technique and collected by a CPU. The lifetimes were obtained with the chopped signal at 20 Hz and a single exponential decay fitting.

Results and Discussion

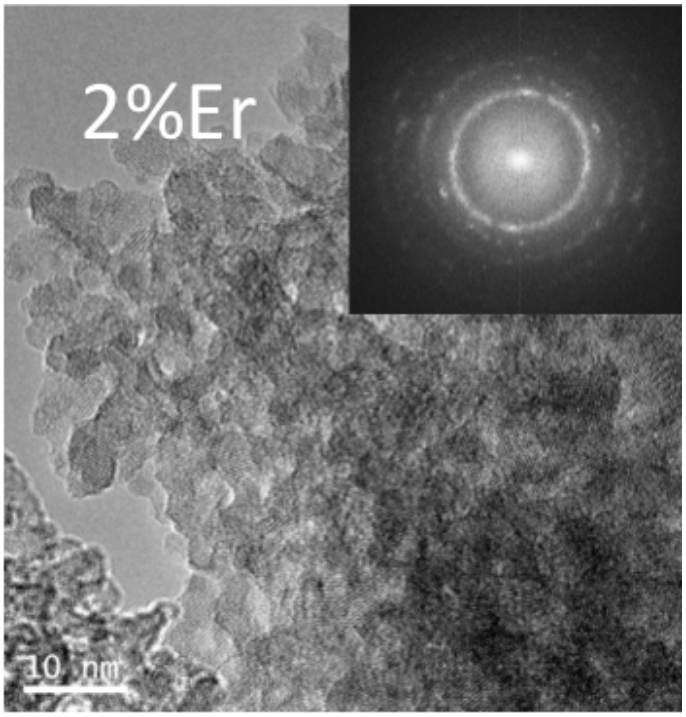

Figure 1. Bright-field TEM image representative of the 2 mol % Er^{3+}-doped TiO_2 nanocrystalline xerogels in the as-prepared condition. The inset shows the corresponding electron diffraction pattern.

Figure 1 shows a representative bright field transmission electron microscopy image of the Er^{3+}-doped TiO_2 nanocrystalline xerogels. The as-prepared xerogels are formed by anatase nanocrystallites with sizes smaller than 7 nm. As discussed in previous work, this result is consistent with the observation of a very broad (101) anatase peak in the corresponding X-ray diffraction (XRD) patterns [14], recently Yurtsever *et al*. [16] reported that for undoped TiO_2 the predominant phase was anatase during thermal

treatments at about 600-700 °C, and up to 900 °C when TiO_2 is doped with wide variety of rare-earth ions, including Er^{3+}.

The samples were studied by Raman spectroscopy to determine the crystalline phase and its evolution as a function of the thermal treatment from 300 to 900 ºC. The Raman spectra for all the studied concentrations (1, 2, and 3% Er), as well as for the undoped reference xerogel as a function of the temperature, are included in the Appendix A in figure A1. It has been found for all the concentrations that up to500 ºC the predominant phase is anatase. As the samples are treated at higher temperatures the features related to the rutile phase start to emerge in the Raman spectra. This tends to appear at higher temperatures as the Er concentration increases, from 700 ºC for the 1% Er-doped sample to 900 ºC for the 3% Er-doped sample. Additionally at the highest temperatures (900 ºC) and Er concentrations of 3% the Raman spectrum shows an additional peak that reveals the formation of the pyrochlore $Er_2Ti_2O_7$ compound [14].

The anatase to rutile transformation of the xerogels as a function of the temperature can be monitored in more detail by analyzing the evolution of the characteristic peaks. In particular, by measuring the ratio of the area of the 399 cm^{-1}peak that is related to the anatase phase (A_a), to the area of the 447 cm^{-1} peak that is related to the rutile (A_r)in each Raman spectrum [17,18]. Previous works by several authors have shown that this area ratio is directly proportional to the relative amount of known anatase and rutile mixtures [19,20,21]. In order to achieve semi-quantitative data first a calibration line was performed by determining the relative ratio $A_{rel} = A_r / (A_r + (\sigma_a/\sigma_r) A_a)$ for each of the series with a given Er molar ratio, where σ_a/σ_r is the cross section ratio of the anatase and rutile crystals, respectively, that can be considered constant.

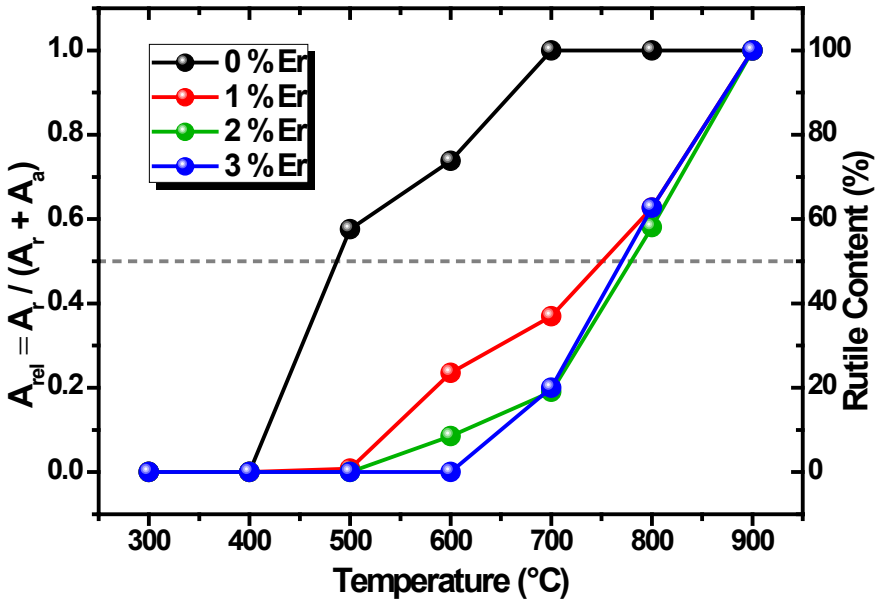

Figure 2. Relative ratio of the rutile to anatase phase in the xerogels (left axis) and rutile phase percentage compared to the anatase (right axis).

Figure 2 shows the obtained relative ratio of the areas of the rutile and anatase peaks for all the studied concentrations as a function of the temperature. For the undoped xerogel the lowest A_{rel} was achieved at 400 ºC, and this was assumed to be 100% anatase. The highest value of the relative intensity ratio is achieved for all xerogels after the thermal treatment at 900 ºC, which was assumed to correspond to the 100 % rutile phase. This assumptions are well correlated and in very good agreement by XRD analysis [14].From the present analysis of the Raman peaks, the estimated onset of the transition from anatase to rutile was found to be between 400–500 ºC for the 0 and 1 % Er, 500–600 ºC for 2 % Er, finally between 600–700 ºC for 3 % Er molar ratio. It is noticeable that the rutile phase tends to form at higher temperature in presence of Er, which stabilizes the anatase phase.

Determination of the xerogels bandgap is important in order to understand their absorption behavior upon photon excitation. Therefore UV-Vis-NIR spectrophotometry analysis was performed in the diffuse reflectance mode, the spectra of the xerogels is

included in the Appendix B in figure B1. The Er absorption peaks are clearly identified, along with the TiO_2 absorption edge related to the optical bandgap. In order to achieve a quantitative insight into the evolution of the TiO_2 effective bandgap, we performed the Kubelka-Munk transformation, F(R),of the diffuse reflectance spectra which is related to the absorption of the xerogels [22,23] and then, by using the Tauc-plot method, we have determined the values of the effective optical bandgap corresponding to the TiO_2 nanocrystals. The Tauc-plot method requires an assumption on the nature of the bandgap of the studied material, direct or indirect; this assumption dictates the way to analyze the optical data. Whereas bulk anatase TiO_2 is known to present an indirect bandgap, it has been suggested that as a result of the quantum confinement the bandgap of TiO_2 increases and it might change its nature from indirect to direct [24,25]. In contrast, the bandgap of rutile TiO_2 is known to be direct already for the bulk material. Therefore, in order to perform a consistent analysis, we have determined the effective optical bandgap of the TiO_2 xerogels assuming that it has a direct nature [24]. Consequently, we have plotted the function $(F(R)*h\nu)^2$ versus $h\nu$, and determined the intersection of the linear slope of the $(F(R)*h\nu)^2$ function in the 3 to 4 eV range with the abscissa axis. Figure 3 shows the calculated optical direct bandgap for the xerogels having 0, 1, 2 and 3 % Er molar ratios as a function of the annealing temperature. For the as-prepared xerogels, the optical bandgap values are slightly higher for the Er-doped xerogels than for the undoped ones, by about 0.15 eV, this might be related to the fact that the nanocrystalline size has shown to be always smaller for the doped xerogels than for the undoped ones [14], thus allowing a stronger bandgap opening due to electronic confinement. In addition, higher values of the bandgap are observed for higher Er concentrations, this may be due to the fact that the fraction of anatase in the xerogel

increases with the Er concentration, and the anatase phase has been reported to have a higher bandgap than rutile phase.

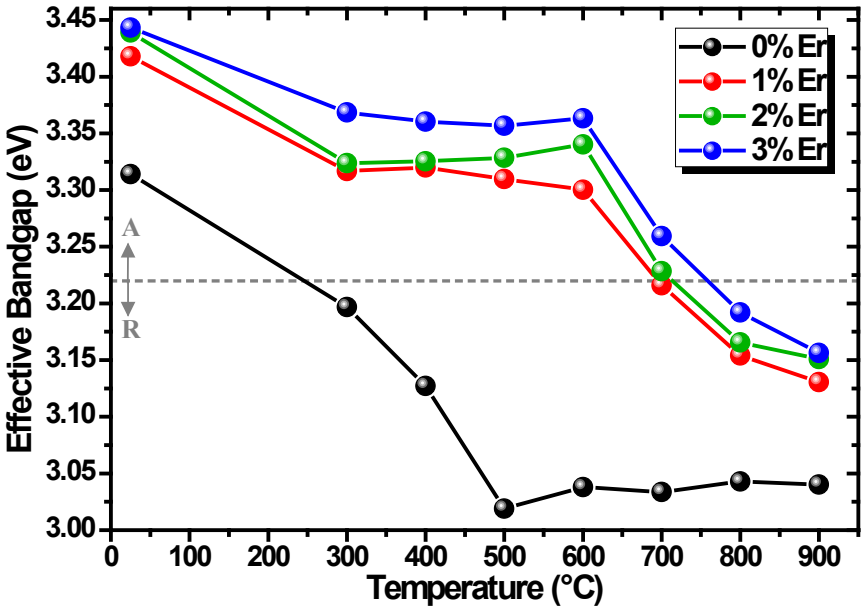

Figure 3. Effective bandgap values for the undoped and 1, 2, 3 % Er doped TiO_2 xerogels. The horizontal dashed line indicates the estimated limit for the optical bandgap between anatase (A) and rutile (R) phases according to Hanaor *et al.*[9]

Figure 3 shows that upon thermal treatment, the obtained values for the optical bandgap of the undoped xerogel nanocrystallites decrease from 3.32 to 3.02 eV as the phase transformation from anatase to rutile progresses. The obtained bandgap values are in good agreement with the literature, where higher bandgap values are seen for anatase when compared with rutile at around 3.3 eV [9,19], and then they show a continuous and fast decrease of the bandgap values that is stabilized after annealing at 500 ºC, coinciding with the formation of the rutile phase as shown in Figure2. However, the evolution of the bandgap values as a function of the temperature for the Er-doped xerogels show a different behavior that is characterized by three differentiated stages. First there is a small decrease up to the annealing at 300ºC that could be related to the diffusion of the Er ions into the anatase lattice together with the increase in crystallite

size that induces a reduction in the bandgap value [14]. Second there is a stabilization of the bandgap values up to 600 ºC that corresponds to the stabilization of the anatase phase with bandgap values around 3.3 eV. Finally, there is a further decrease after the annealing at 600ºC that according to the results in Figure2 corresponds to the beginning of the formation of rutile phase that has a lower bandgap value, until at 900 ºC most of the xerogel nanocrystals are in the rutile phase with a bandgap value around 3.15 eV. The good correlation between the evolution of our empirical optical bandgap values and that of the xerogel nanocrystallites structure upon doping and annealing suggests the adequacy of assuming a direct bandgap, especially for tracking the anatase to rutile phase transition.

Thus far we have seen that the presence of the Er is able to stabilize the anatase phase as the main phase up to 700ºC. However, up to this point we have been analyzing the response of the nanocrystals structure and its properties. In the following, we will focus on the understanding of the Er emission and its relationship with its local environment.

Optical emission. Photoluminescence.

In order to access to qualitative information on the local Er environment, first we start by studying the Er visible emission excited with infrared light. Since the electronic levels of the Er^{3+} responsible for the visible emissions are located at higher energies they suffer greater influence by the local Er^{3+} environment due to the crystal field of the matrix than the innermost ground transitions in the infrared [7]. In order to observe the changes in the visible transitions of Er^{3+} we have excited the xerogels with infrared light at 980 nm. Figure 4 shows the resulting visible upconversion-induced PL spectra for the 1% Er-doped xerogels obtained after the annealing at 500, 600, 700, 800 and 900 ºC. Below 500 ºC no upconversion emission signal could be recorded.

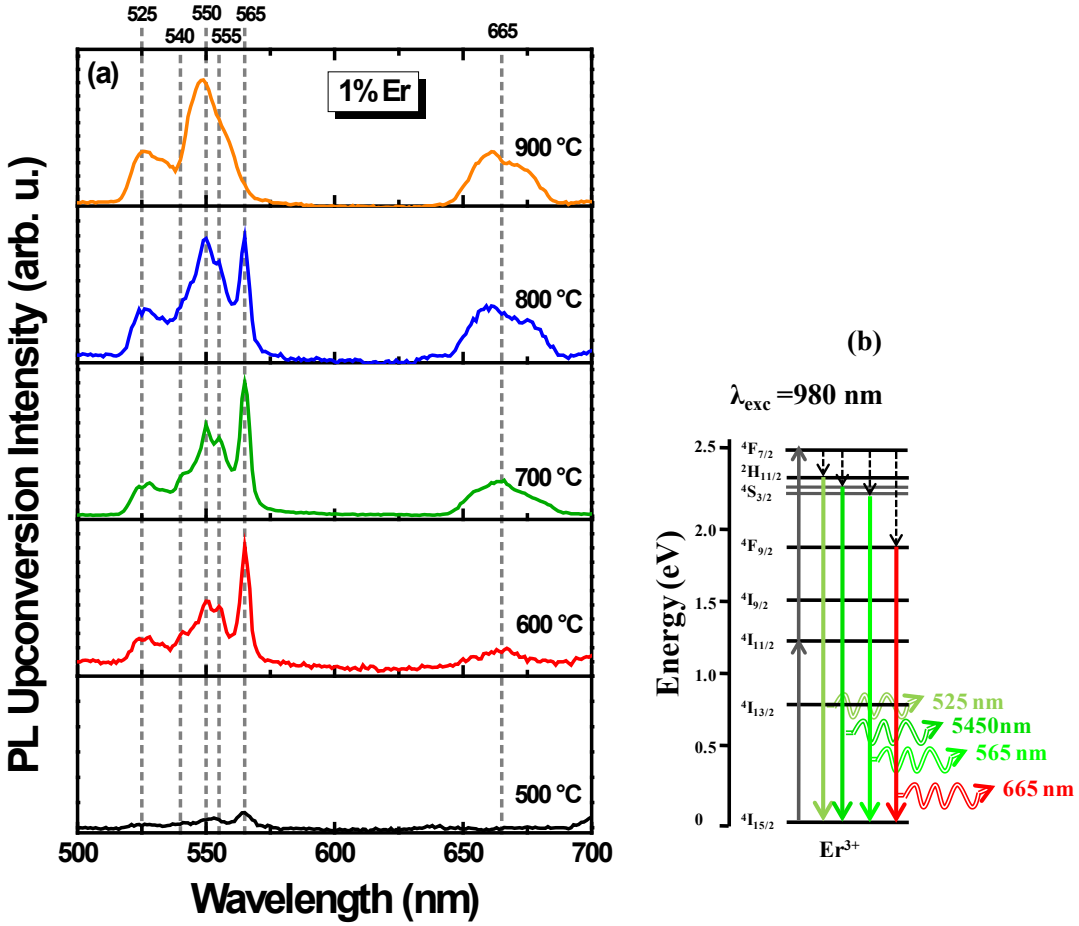

Figure 4. (a) Upconversion-induced visible photoluminescence spectra under near-infrared excitation (at 980 nm) of a xerogel containing 1 % Er for the different thermal treatments.(b) Schematic energy diagram of the upconversion-PL process under NIR excitation.

After the treatment at 500 ºC there is a weak and broad visible emission bands with maxima around 525, 555 and 565 nm. At this stage Er^{3+} ions should be mostly in the vicinity of the anatase crystal lattice according to figure 2, and nevertheless it is found that the upconversion signal is still inefficient, indicating that still many Er ions are not participating in the upconversion light emission. After annealing at 600 ºC these bands are finally better defined and show some clear splitting, for example, the band around 550 nm is formed by three peaks at 540, 550 and 555 nm. Additionally a band at 665 nm becomes clearly visible. This spectrum is fully consistent with that recently reported for upconversion of Er-doped anatase TiO_2[7]. The emission in the spectral 520–535 nm

region is ascribed to the $^2H_{11/2} \rightarrow {}^4I_{15/2}$ transition, and that of the 535–575 nm region is attributed to the $^4S_{3/2} \rightarrow {}^4I_{15/2}$ transitions of Er^{3+}. The weaker red emission in the 640–700 nm region corresponds to the $^4F_{9/2} \rightarrow {}^4I_{15/2}$ transition [7]. Nevertheless, after the annealing temperature is increased to 700 and 800 ºC the relative intensity of the peaks in the spectra changes: the intensity of the peak at 565 nm decreases and that of the peaks located around 525, 550 and 665 nm increases. In addition, the position of the bands around 550 and 665 nm present a slight shift to lower wavelengths and the maxima are found around 548 and 660 nm. Finally, at 900 ºC the peak at 565 nm disappear, as well as the minor peaks at 540 and 555 nm. The new spectral shape shows quite broad peaks with two maxima corresponding to the green emission, at 525 and 548 nm, and two for the red emission at approximately 660 and 670 nm.

Similar evolution for the green upconversion emission excited at 980 nm was found by Zhang *et al*. for Er:TiO_2 doped nanocrystals [26]. They found well defined emission peaks dominated by the 565 nm emission for temperatures up to 800 ºC, while after the treatment at 900ºC the green spectrum was much broader and dominated by the 550 nm emission. It is very interesting to note that they characterized structurally the nanocrystals by XRD and they were able to clearly ascertain the formation of the pyrochlore $Er_2Ti_2O_7$ compound after the treatment at 800 ºC and coexisting with the anatase phase. After the treatment at 900 ºC they reported an increase of the pyrochlore compound coexisting with the rutile phase that completely replaces the anatase phase. Patra *et al*. [27] also reported upconversion emissions of Er^{3+} in TiO_2 as a function of temperature, and after the treatment at 800 ºC the upconversion spectra in their samples also show an increase of the 550 nm emission, while the 565 nm emission peak clearly visible after the 500 ºC annealing decreases, and finally completely disappears after their 1000 ºC treatment. From XRD analysis they also report the formation of the

pyrochlore compound after their 1000 ºC treatment. Therefore from our observations, and correlating them with the results by Zhang and Patra [26,27], we conclude that the green emissions at 540, 555, 565 nm are most likely associated to Er^{3+} ions embedded as solid solution in anatase crystals, and therefore they are clearly visible in the 600-700 ºC spectra, and tend to decrease at higher temperatures. Note that figure 2 suggests that up to 800 ºC there is still a 40% fraction of anatase and this is consistent with the fact that Er-related anatase emission is clearly observed in the 800 ºC spectrum of figure 4. Concerning the other bands, it is difficult to ascribe them to a specific Er^{3+} local environment because they are always present through the phase transformations; however they show clearly different shapes [7,26]. Among them it is remarkable the green band peaking at 550 nm that dominates the spectrum after the 900 ºC treatment, thus representative of the Er^{3+} emission after the TiO_2 xerogels are fully transformed into a mixture of rutile phase and pyrochlore $Er_2Ti_2O_7$ compound. Therefore we suggest that this wide emission might be related to the emission of Er^{3+} ions in the pyrochlore $Er_2Ti_2O_7$ compound. We will come to this result again in the following section, once we discuss the infrared emission. In order to picture the evolution of the Er^{3+} local environment as a function of the temperature in figure 5 we have plotted the ratio of the 550 to565 nm emissions (both related to the $^4S_{3/2} \rightarrow {}^4I_{15/2}$ transition) versus temperature.

Up to 700 ºC the slope of the emissions ratio as a function of the temperature is very small, indicative of a negligible change of the Er^{3+} local environment. Only after 800 ºC the slope shows a sharper increase indicative of strong change of Er^{3+} ions emission characteristics. It is interesting to note that this behavior is somewhat different from that shown for this film for the structural anatase to rutile transformation in figure 2, where a progressive transformation is clearly observed starting at 500 ºC and progressing as the

temperature increases; not such a gradual change is shown in figure 5 suggesting that the Er local environment is very similar up to 700 ºC.

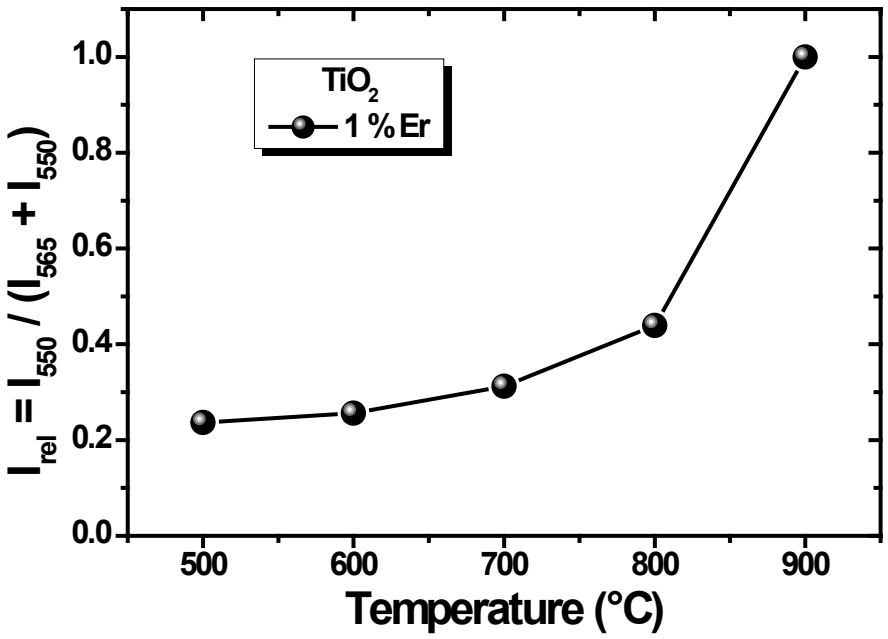

Figure 5. Intensity relation between emissions from the $^4S_{3/2} \rightarrow {}^4I_{15/2}$ transition, as a function of the temperature for the 1% Er-doped TiO_2 xerogel.

Now, in the following we complete our study by analyzing the Er^{3+} infrared emission excited with visible light (488 nm) that is related to the innermost 4f transitions from the first excited manifold of Er $^4I_{15/2}$ to the ground manifold $^4I_{13/2}$.

Figure 6 shows the infrared PL spectra corresponding to the 1% Er-doped $TiO_2$for as-prepared xerogels and after 1 hour of thermal treatment at 500, 700, 800 and 900 ºC. The spectra have been obtained under excitation at 488 nm. The corresponding PL spectra for the lower annealing temperatures (300 and 400 ºC) and the other Er concentrations (2 and 3 % Er) have been included in the Appendix C in figure C1. In this case a clear emission spectra for the as-prepared xerogels is observed, the spectrum shows a wide broad band with a maximum around 1530 nm and a shoulder towards long wavelengths. These broad emission spectra are characteristic of Er^{3+} ions embedded in a heterogeneous environment in which each Er^{3+} ion experiences a

different crystal field, and have been typically reported for Er^{3+} embedded in amorphous matrices [28].

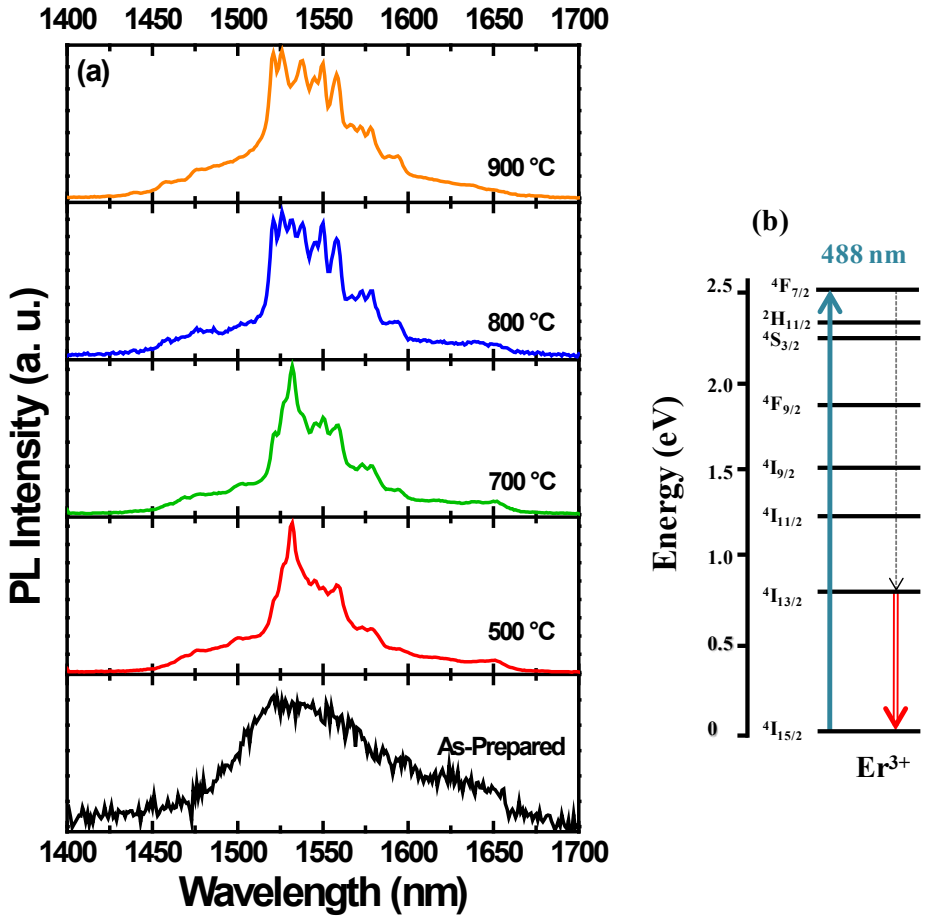

Figure 6. (a) Photoluminescence spectra, under excitation at 488 nm, of Er^{3+} doped TiO_2 xerogels with 1% Er molar ratio for the as-prepared and different temperatures. (b) Schematic energy diagram of the NIR-PL process under visible excitation.

However from the structural characterization in this work and in previous works [12,14] it has been determined that the TiO_2 xerogels are formed by nanostructures mainly crystallized in the anatase phase and no amorphous phases have been identified. Therefore since the Er^{3+} ions are not located in well-defined positions within the anatase crystalline lattice, most likely they are adsorbed at the surface of the nanocrystals. This is in agreement with previous results of zeta potential measurements in the sols [12].

This is a consequence of the formation of the nanocrystals following a thermodynamic equilibrium process that leads to the segregation of the Er^{3+} ions to the crystallite surface due to their larger ionic radius compared to that of Ti^{4+} ions. This is the first evidence that the local environment of Er ions is not necessarily that of the main crystalline phase of the TiO_2 xerogels.

Upon thermal treatment the PL intensity and shape changes significantly, as shown in figure 6 for the 1% Er-doped xerogel (See figure C1 for the other concentrations). The increase in PL (shown in figure C2) is mainly related to the decrease of –OH groups content (see fig. B1). More interesting is to discuss the change in the PL spectral shape. Starting with the 300 and 400 ºC treatments (figure C1), and more clearly for the 500 ºC annealing, there is a sharpening of the emission and several peaks can be distinguished as shown in figure 6(a), where a peak with the maximum at 1532 nm is now clearly identified. The observed spectrum is a result of the sharp emission peaks coming from the transitions from the first excited manifold of Er $^4I_{13/2}$ to the ground manifold $^4I_{15/2}$ (see figure 6(b)). The drastic change of the emission shape is most likely due the coarsening of the smaller TiO_2 nanocrystals forming larger ones [14], and forcing the Er^{3+} ion to start occupying more ordered positions within the TiO_2 lattice. In general, when the Er^{3+} ions are incorporated into a crystalline lattice it is expected that they experience a similar crystal field and therefore show the emission at well-defined wavelengths corresponding to the transitions of the different manifolds [7,29]. Indeed, detailed spectroscopic analysis performed in Er-doped TiO_2 anatase nanocrystals prepared by a sol-gel solvothermal method combined with crystal field calculations has shown that the Er^{3+} ions tend to occupy a single type of lattice site. The symmetry of this position is of type C_{2v} and it is compatible with a structural distortion of the anatase lattice due to the large ionic radius of the Er^{3+} ions compared to the Ti^{4+} ions [7,29].

Therefore, according to the shape of the spectra of fig. 6(a) after 500 ºC, we can conclude that Er^{3+} ions are mainly incorporated in the anatase lattice in well-defined positions, which falls in perfect agreement with the observed tendency through upconversion.

As the temperature of the treatments increases, as in fig. 6(a) after the 700 ºC, and especially for the 800 and 900 ºC treatments, it can be seen that the PL spectral shape changes significantly. The spectra show many well defined peaks in the spectral region from 1500 to 1600 nm, that after the annealing at 800 and 900 ºC exhibit a similar intensity than the peak at 1532 nm. However note that for this C_{2v} site the crystal field (CF) splitting of level $^4I_{15/2}$only into 8 sublevels is expected. In fact in earlier reports(i.e. Bahtat *et al*. [30]) the spectral shape is similar to that reported in our work, however fewer peaks are usually observed. The splitting in a higher number of peaks could be related the location of part of the Er ions in other additional crystalline positions, and is consistent with those reported for the infrared emission of Er^{3+} in pyrochlore compound $Er_2Ti_2O_7$ films [30,31]. Note that this is not in contradiction with the fact that the main phase of the TiO_2 at 800 ºC is rutile, as the pyrochlore is only a minority phase that requires the presence of Er in its composition. Therefore, from the PL spectra shown in figure 6(a) we can conclude that after the annealing at 800 ºC the Er^{3+} ions are mainly in a pyrochlore environment. In fact a detailed observation of the spectra in figure 6 and figure C1 suggests that even after the annealing at 600 ºC some Er^{3+} ions might be already in a pyrochlore environment, since small peaks of this characteristic emission can be observed. At this point we can come back to our results from visible upconversion spectra, and it can be confirmed that indeed the wide green band peaking at 550 nm that dominates the visible spectrum after the 900 °C annealing is most likely related to the pyrochlore phase.

Earlier reports studied the anatase-to-rutile phase transition and formation of the pyrochlore compound $Er_2Ti_2O_7$, either by Raman and/or XRD analysis at the highest annealing temperatures [14,16], nonetheless, in the present work we have shown that by means of the PL we are able to detect the formation of the pyrochlore compound at a relatively low temperature, in the 600-700 °C treatment. Which is in agreement with Zhang *et al*. [18] that studied the anatase to rutile phase transition through Raman spectroscopy, and determined that this transition occurred at the top-surface of the material, which might indicate that the pyrochlore compound is therefore formed preferentially at the surface of the nanocrystals since the Er^{3+} ions are segregated from the rutile structure [9]. If we go back now to the visible upconversion emission spectra on figure 4 we can conclude that as suggested previously the spectra observed at 900 ºC most likely corresponds to the emission of Er^{3+} ions in a pyrochlore environment; the PL infrared results indicate that this compound starts to form at earlier annealing stages, and Er can be coexisting in anatase and pyrochlore environments at temperatures as low as 600 ºC. The combined analysis of the visible and infrared Er^{3+} ions emission seems to suggest that as a function of the temperature our TiO_2 xerogels the Er^{3+} ions are mainly in two preferential sites, one before the treatment at 700 ºC and another after the annealing at 800 ºC. Before the 600-700ºC treatment they are preferentially in a solid solution within the anatase phase, and after the 700-800 ºC annealing they are preferentially forming part of the pyrochlore structure. In the supplementary material in figure C1 it can be seen that the pyrochlore is formed at higher temperatures as the Er concentration increases and therefore it is not observed up to 900 ºC for the 2 and 3% Er concentrations. This is in good agreement with the fact that the phase transition to rutile is retarded and therefore, until the segregation of Er due to the formation of the rutile phase occurs, no formation of pyrochlore is observed.

Conclusions

Nanoparticulate colloidal xerogels of TiO_2 doped with Er at 1, 2 and 3 % molar ratio have been successfully produced; the as-prepared xerogels are formed by anatase nanocrystallites with sizes smaller than 7 nm. The incorporation of Er^{3+} ions in anatase can be clearly identified observing the evolution of the characteristic features of PL visible upconversion and infrared Er^{3+}emissions as a function of the thermal treatment temperature. Upon thermal treatment the Er^{3+}-doped TiO_2 colloidal xerogels exhibit slower kinetics of anatase-to-rutile phase transformation compared to the undoped ones, and anatase nanocrystallites are preserved up to 800 ºC as a consequence of the incorporation of the Er^{3+} ions in the anatase TiO_2 lattice. The size of the Er^{3+}-doped nanocrystals is smaller compared to the undoped nanocrystals resulting in larger optical bandgap values. According to the structural analysis up to 700 ºC nanocrystals both in anatase and rutile phases coexist and, finally after 800 ºC the rutile TiO_2 phase and pyrochlore $Er_2Ti_2O_7$ compound co-exist. While structural analysis techniques, such as Raman and XRD, show the formation of the pyrochlore phase only at high temperature, the well-defined peaks of the infrared PL spectra evidence that the active Er^{3+} ions could be forming part of the pyrochlore nanocrystal lattice at temperatures as low as 600 ºC depending on Er concentration. Furthermore, these results suggest that the pyrochlore compound might be formed preferentially at the surface of the nanocrystals since it is formed as a result of Er^{3+} ions segregation out of the main rutile structure. The presence of the pyrochlore phase at the nanocrystals surface and co-existing with the anatase phase might be relevant for applications such as photo-induced catalysis that has been so far underestimated. These results show the potential of the optical characterization and specifically of the combined analysis of PL emissions both in the infrared and visible ranges as a probe of the structural properties of the Er-doped TiO_2

nanocrystalline phases. The presence of Er^{3+} active phases makes this technique more sensitive than XRD and Raman to the determination of crystalline phases. In this work PL measurements have shown to be useful to only to observe the phase transitions in the TiO_2 material, but also have helped to identify Er ions in-diffusion and segregation phenomena.

Acknowledgements

This work was supported by the Ministerio de Economía y Competitividad (MINECO, Government of Spain) under Grants MINECO/FEDER TEC2015-69916-C2-1-R and MAT2015-65356-C3-1-R. IC and MB acknowledge the grants JAE-Pre-201100578 and JAE-Pre-083, respectively.

References

[1] M. Chang, Y. Song, Y. Sheng, J. Chen, H. Guan, Z. Shi, X. Zhou, K. Zheng, H. Zou, Photoluminescence and photocatalysis properties of dual-functional Eu^{3+}-doped anatase nanocrystals, J. Phys. Chem. C121(4) (2017) 2369–2379.

[2] M. Jiang, C. Zhu, J. Zhou, J. Chen, Y. Gao, X. Ma, D. Yang, Electroluminescence from light-emitting devices with erbium-dopedTiO_2 films: Enhancement effect of yttrium codoping, J Appl. Phys. 120 (2016) 163104.

[3] J.D.B. Bradley, M.Pollnau, Erbium-doped integrated waveguide amplifiers and lasers, Laser Photon. Rev. 5 (2011) 368–403.

[4] A. Polman, F.C.J.M. van Veggel, Broadband sensitizers for erbium-doped planar optical amplifiers: review, J. Opt. Soc. Am. B 21 (2004) 871.

[5] Y. Yang, Y. Li, L. Jin, X. Ma, D. Yang, Light-emitting devices based on erbium-doped TiO_2/p +-Si heterostructures: Engineering of electroluminescence via aluminum co-doping, Appl. Phys. Lett. 102 (2013) 021108.

[6] E.F. Pecora, T.I. Murphy, L. Dal Negro,Rare earth doped Si-rich ZnO for multiband near-infrared light emitting devices, Appl. Phys. Lett. 101 (2012) 191115.

[7] W. Luo, C. Fu, R. Li, Y. Liu, H. Zhu, X. Chen, Er^{3+}-doped anatase TiO_2 nanocrystals: Crystal-field levels, excited-state dynamics, upconversion, and defect luminescence, Small 7 (2011) 3046.

[8] J. Albiol, J. Cerdà, G. Dezanneau, A. Cirera, F. Peiró, A. Cornet, J.R. Morante, Effects of Nb doping on the TiO_2 -rutile phase transition, J. Appl. Phys. 92 (2002) 853.

[9] D.A.H. Hanaor, C.C. Sorrell, Review of the anatase to rutile phase transformation, J. Mater. Sci. 46 (2010) 855–874.

[10] G.C. Vasquez, M.A. Peche-Herrero, D. Maestre, A. Gianoncelli, J. Ramírez-Castellanos, A. Cremades, J.M. Gonzalez-Calbet, J. Piqueras, Laser-induced anatase-to-rutile transition in TiO_2 nanoparticles: promotion and inhibition effects by Fe and Al doping and achievement of micropatterning, J. Phys. Chem. C 119(21) (2015) 11965–11974.

[11] Y. Zhang, H. Zhang, Y.Xu, Y. Wang, Significant effect of lanthanide doping on the texture and properties of nanocrystallinemesoporous TiO_2, J. Solid State Chem. 177 (2004) 3490–3498.

[12] M. Borlaf, M.T. Colomer, F. Cabello, R. Serna, R. Moreno, Electrophoretic deposition of TiO_2/Er^{3+}nanoparticulate sols, J. Phys. Chem.B 117(2013) 1556−1562.

[13] I. Camps, M. Borlaf, M. T. Colomer, R. Moreno, L. Duta, C. Nita, A. Perez del Pino, C. Logofatu, R. Serna and E. György, Structure-property relationships for Eu doped TiO2 thin films grown by a laser assisted technique from colloidal sols, RSC Advances, 2017, 7, 37643.
[14] M. Borlaf, M.T. Colomer, R. Moreno, A.L. Ortiz, Effect of Er^{3+} doping on the thermal stability of TiO_2nanoparticulatexerogels, J. Nanopart. Res. 15 (2013) 1752.
[15] M. Borlaf, M.T. Colomer, R. Moreno, A. de Andres, Structural and photoluminescence study of Eu^{3+}/TiO_2 xerogels as a function of the temperature using optical techniques, J. Am. Ceram. Soc. 98 (2015) 338–345.
[16] H.A. Yurtsever, M. Çiftçioğlu, The effect of rare earth element doping on the microstructural evolution of sol-gel titania powders, J. Alloys Compd. 695 (2017) 1336-1353.
[17] Enrique Camps, V.H. Castrejón-Sánchez, Marco A. Camacho-López, R. Basurto, Influence of the nitriding process on the band-gap of TiO_2 thin films with phase mixture, Thin Solid Films 581 (2015) 54-58.
[18] J. Zhang, M. Li, Z. Feng, J. Chen, C. Li, UV Raman spectroscopic study on TiO_2. I. Phase transformation at the surface and in the bulk, J. Phys. Chem. B 110 (2006) 927-935.
[19] W. Ma, Z. Lu, M. Zhang, Investigation of structural transformations in nanophase titanium dioxide by Raman spectroscopy, Appl. Phys. A 66 (1998) 621-627.
[20] F.D. Hardcastle, Raman spectroscopy of titania (TiO_2) nanotubular water-splitting catalysts, J. Ark. Acad. Sci. 65 (2011) 43.
[21] I.M. Clegg, N.J. Everall, B. King, H. Melvin, C. Norton, On-Line analysis using Raman Spectroscopy for process control during the manufacture of titanium dioxide, Appl. Spectrosc. 55 (2001) 1138.
[22] L. Yang, B. Kruse, Revised Kubelka–Munk theory. I. Theory and application, J. Opt. Soc. Am. A 21 (2004) 1933-1941.
[23] L. Yang, S.J. Miklavcic, Revised Kubelka–Munk theory. III. A general theory of light propagation in scattering and absorptive media, J. Opt. Soc. Am. A 22 (2005) 1866-1873.
[24] K.M. Reddy, S.V. Manorama, A.R. Reddy, Bandgap studies on anatase titanium dioxide nanoparticles, Mater. Chem. Phys. 78 (2002) 239-245.
[25] N. Serpone, D. Lawless, R. Khairutdinov, Size effects on the photophysical properties of colloidal anatase TiO_2 particles: size quantization versus direct transitions in this indirect semiconductor? J. Phys. Chem. 99 (1995) 16646-16654.
[26] J. Zhang, X. Wang, W.T. Zheng, X.G. Kong, Y.J. Sun, X. Wang, Structure and luminescence properties of TiO_2:Er^{3+} nanocrystals annealed at different temperatures, Mater. Lett. 61 (2007) 1658–1661.
[27] A. Patra, C.S. Friend, R. Kapoor, P.N. Prasad, Fluorescence upconversion properties of Er^{3+}-doped TiO_2 and $BaTiO_3$ nanocrystallites. Chem. Mater. 15 (2003) 3650-3655.
[28] S. Núñez-Sánchez, P.M. Roque, R. Serna, A.K. Petford-Long, Si nanoparticle–Er^{3+} coupling through contact in as-deposited nanostructured films, Appl. Phys. Lett. 98 (2011) 151109.
[29] Y. Liu, W. Luo, H. Zhu, X. Chen, Optical spectroscopy of lanthanides doped in wide band-gap semiconductor nanocrystals, J. Lumin.131 (2011) 415-422.
[30] A. Bahtat, M. Bouazaoui, M. Bahtat, J. Mugnier, Fluorescence of Er^{3+} ions in TiO_2 planar waveguides prepared by a sol-gel process, Opt. Commun. 111 (1994) 55-60.
[31] M. Langlet, C. Courtier, J. Fick, M. Audier, W. Meffre, B. Jacquier, R. Riment, Sol–gel thin film deposition and characterization of a new optically active compound: $Er_2Ti_2O_7$, Opt. Mat. 16 (2001) 463-473.